energies

MDPI

Article

Heterogeneity of a Sandy Conglomerate Reservoir in Qie12 Block, Qaidam Basin, Northwest China and Its Influence on Remaining Oil Distribution

Qingshun Gong [1], Zhanguo Liu [1], Chao Zhu [1,*], Bo Wang [2], Yijie Jin [3], Zhenghao Shi [2], Lin Xie [2] and Jin Wu [1]

[1] PetroChina Hangzhou Research Institute of Geology, Hangzhou 310023, China; gongqs_hz@petrochina.com.cn (Q.G.); wuj_hz@petrochina.com.cn (J.W.)
[2] Exploration and Development Institute of Qinghai Oilfield Company, CNPC, Dunhuang 736202, China
[3] China National Logging Company, Beijing 100101, China
* Correspondence: zhuc_hz@petrochina.com.cn; Tel.: +86-531-8522-4934

Abstract: In view of the key geological factors restricting reservoir development, the reservoir heterogeneity of an alluvial fan sandy conglomerate reservoir in the Qie12 block of Qaidam Basin, Northwest China, and its influence on remaining oil distribution, were studied according to geology, wireline logging data, and dynamic production data. This study illustrates that the difference in pore structures, which are controlled by different sedimentary fabrics, is the main cause of reservoir microscopic heterogeneity. Besides, the temporal and spatial distribution of architectural units in the alluvial fan controls reservoir macroheterogeneity. Our results show that the thick sandy conglomerate develops two types of pores, two types of permeability rhythms, two types of interlayers, two types of interlayer distribution, two types of effective sand body architecture, and four types of sand body connecting schemes. The strongest plane heterogeneity is found in the composite channel unit formed by overlapping and separated stable channels of the middle fan, and the unit's permeability variation coefficient is >0.7. However, the variation coefficient in the range of 0.3–0.5 is found in the extensively connected body unit sandwiched with intermittent channels of the inner fan. The distributions of the remaining oil vary significantly in different architectural units because of the influence of reservoir heterogeneity, including distribution patterns of flow barriers, permeability rhythm, and reservoir pore structures. The composite channel unit formed by overlapping and separated stable channels, or the lateral alternated unit with braided channel and sheet flow sediment of the middle fan, is influenced by the inhomogeneous breakthrough of injection water flowing along the dominant channel in a high-permeability layer. The microscopic surrounding flow and island-shaped remaining oils form and concentrate mainly in the upper part of a compound rhythmic layer. Meanwhile, in the extensively connected body unit sandwiched with intermittent channels of the inner fan, poor injector–producer connectivity and low reservoir permeability lead to a flake-like enrichment of the remaining oil.

Keywords: reservoir heterogeneity; remaining oil; sandy conglomerate reservoir; alluvial fan; Qaidam Basin

Citation: Gong, Q.; Liu, Z.; Zhu, C.; Wang, B.; Jin, Y.; Shi, Z.; Xie, L.; Wu, J. Heterogeneity of a Sandy Conglomerate Reservoir in Qie12 Block, Qaidam Basin, Northwest China and Its Influence on Remaining Oil Distribution. *Energies* **2023**, *16*, 2972. https://doi.org/10.3390/en16072972

Academic Editor: Dameng Liu

Received: 14 February 2023
Revised: 11 March 2023
Accepted: 22 March 2023
Published: 24 March 2023

1. Introduction

Reservoir heterogeneity is the term used to describe the uneven alternations in spatial distribution and internal attributes, which are caused by the influences of sedimentary environments, diagenetic processes, and tectonism during the formation of oil and gas reservoirs [1–3]. It is an important content of reservoir characterization manifested in both macroscale (plane, intrabedding, and interbedding) and microscale (pore space and structure). Additionally, it is the main geological factor determining the reservoir quality, which constricts the adjustment of a reservoir development scheme and affects the distribution of the remaining oil [4–6].

Conglomerate reservoirs are widely distributed, and they include the Permian–Triassic succession on the northwest edge of Junggar Basin, China; Paleogene Shahejie Formation of Dongying Depression, China; Yingcheng Formation of Songliao Basin, China; Barrancas Formation of Mendoza area, Argentina; and Upper Morrow in Anadarko Basin and Bend Conglomerate in Boonsville Gas Field of Fort Worth Basin, USA [7–12]. In general, they are strongly heterogeneous because of depositional and diagenetic alternations; however, their main controlling factors and specific characteristics on the macrolevel and microlevel are different. In this study, the research area is the Qie12 block in Qaidam Basin, which is a typical sandy conglomerate reservoir. Qie12 block was put into production according to the "thick massive reservoir" geological model during the initial stage of its development; however, the model caused prominent problems such as rapidly declining productivity, quickly declining water volume fraction, uneven injection production, and unclear law of remaining oil distribution. Although research on the characteristics of its sandy conglomerate reservoir has been reported [13], studies on its reservoir heterogeneity have not been conducted. Therefore, this study deeply analyzed the heterogeneous characteristics of Qie12 block's sandy conglomerate reservoir according to geology, logging data, and dynamic production data and determined their influence on the distribution of remaining oil in the research area. On the basis of the results, we provide a theoretical basis for establishing the potential of remaining oil and comprehensive reservoir management.

2. Geological Background

The research area is the Qie12 block, which is located in the Kunbei oilfield of the Qaidam Basin, northwest China. Kunbei oilfield is composed of several tertiary oil-bearing structures, and it is located specifically in the Kunbei fault step zone on the western depression of the Qaidam Basin. Meanwhile, the Kunbei fault step zone is distributed in front of the East Kunlun structural belt, and it is developed by compression from the East Kunlun Mountain to the basin. It has a large piedmont compression torsional thrust structural belt and shows a structural pattern of north–south zoning and east–west blocking [14,15]. In particular, the Qie12 block reservoir is distributed on the west side of the step zone, whereas the block's structural form is an anticline, and its axis is NNE (Figure 1). The lower member of the Ganchaigou Formation (E_3^1), comprising four oil groups, I, II, III, and IV (from top to bottom of Figure 1), was deposited during the Paleogene. In this study, the target layer is oil group IV, which has an average thickness of 55 m and is subdivided into seven small layers.

In the research area, the dominant colors of sediments are brown and brown–red, which are oxidation colors reflecting the characteristics of near-source and rapid accumulation. Meanwhile, the area's sandy conglomerate reservoir shows low composition and structure maturity. The two main types of hydrodynamic mechanisms affecting the area's bedding structure, which can be further used for representing the sedimentary environment, are traction current and gravity flow. The traction current resulted in tabular crossbedding, trough crossbedding, scouring–filling structure, parallel bedding, and gravel orientation structures (Figure 2a–d), whereas the massive bedding and matrix-supported suspended gravel structure were formed by the gravity flow (Figure 2e–g). The lithology types in the block include conglomerate, glutenite, pebbly coarse–fine sandstone, siltstone, pebbly sandstone, and mudstone. We defined eight lithofacies within this study area according to bedding structures, and their characteristics and genesis are summarized in Table 1.

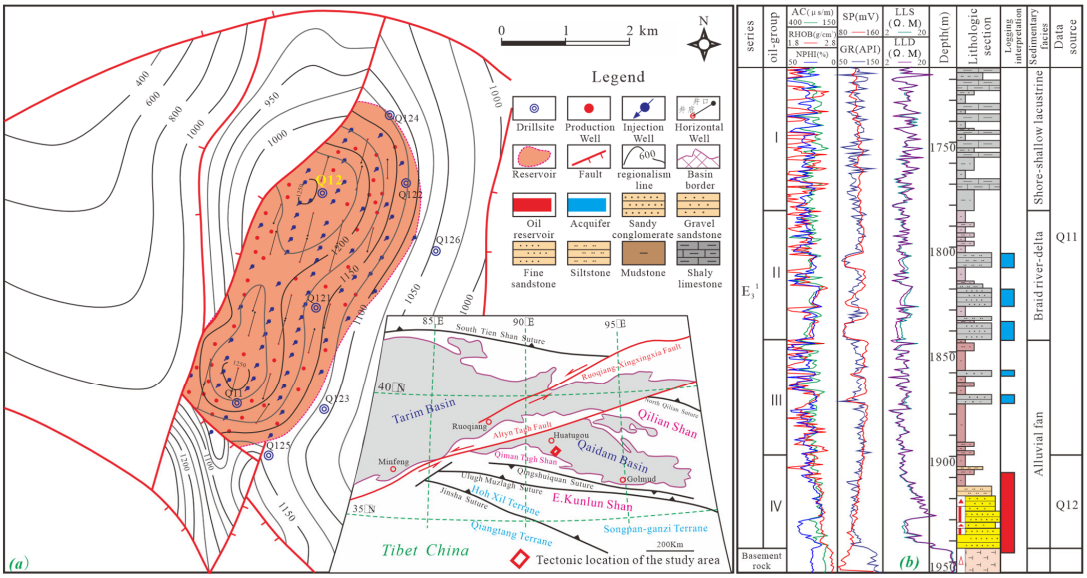

Figure 1. (**a**) Tectonic location of the research area, which is marked with a red box, is the west block of the Kunbei thrust structural belt. (**b**) Diagram showing the composite columnar of the reservoir, where oil layers are concentrated at the bottom of the target stratum. There are six lithofacies and two types of logging interpretation conclusions along the target stratum.

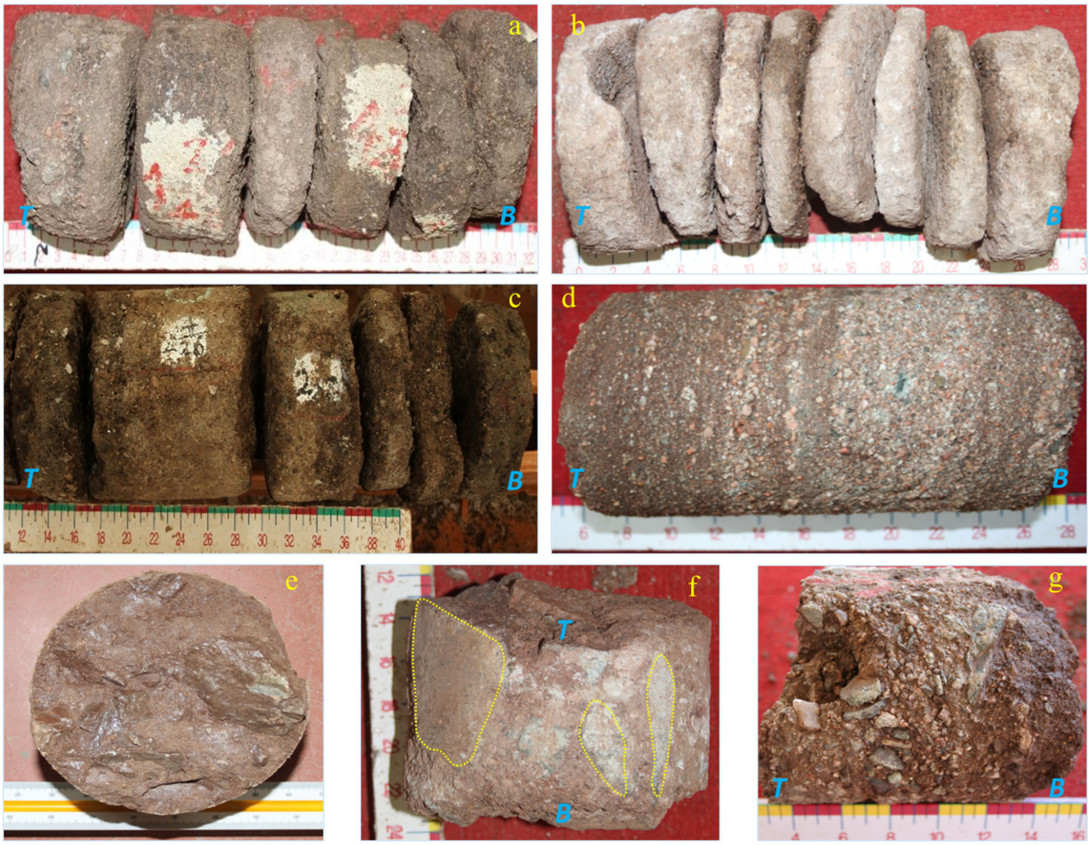

Figure 2. Typical sedimentary structures charts found in the Qie12 block: (**a**) Q12−10−8, 2059.1 m, tabular crossbedding; (**b**) Q12−7−28, 1829.4 m, tabular crossbedding; (**c**) Q12p1, 1809 m, tabular crossbedding; (**d**) Q125, 2026.5 m, trough crossbedding, gravel orientation arrangement; (**e**) Q12−23−6, 1917 m, massive bedding, gravel upright; (**f**) Q12−7−28, 1842.4 m, massive bedding, gravel upright; and (**g**) Q121, 1842.7 m, massive bedding. *T* is the top surface, and *B* is the bottom surface of the core in these figures.

Table 1. Characteristics and genesis of the lithofacies in the Qie12 block.

Code	Lithology Type	Bedding Structure	Genesis	Amplitude Difference of SP Curve	RHOB (g/cm^3)	GR (API)
Gmm	Argillaceous conglomerate–glutenite	Massive bedding, matrix support	Debris flow/sheet flow	moderate	2.36–2.57	85–117
Gei	Sandy conglomerate–glutenite	Massive bedding, grain support, gravel orientation arrangement	Braided channel floor lag	large	2.36–2.57	85–100
Gt	Sandy conglomerate–glutenite	Trough crossbedding	Braided channel-filled deposit	large	2.36–2.57	73–105
Gp	Sandy conglomerate–glutenite	Tabular crossbedding	Braided channel-filled deposit	large	2.36–2.57	73–105
St	Pebbly sandstone	Trough crossbedding	Braided channel-filled deposit	large	2.23–2.44	73–105
SSh	Siltstone	Parallel bedding	Abandoned channel/silted channel deposit/runoff channel	large	2.23–2.44	73–105
Sm	Anisometric sandstone	Massive bedding	Sheet flow/runoff channel	moderate	2.23–2.44	80–125
Mm	Sandy mudstone	Massive bedding, flat bedding	Flood plain	small	1.75–2.41	100–125

By integrating the aforementioned geological features, we believe that the Qie12 block is an alluvial fan, which is a genetic type of thick sandy conglomerate. In the alluvial fan, there are five sedimentary microfacies: a fourth-order architectural element [16] that includes a braided channel, debris flow, sheet flow, runoff channel, and flood plain. According to the vertical assemblage of different architectural elements and the distribution pattern of interlayers [17,18], we also identify four fifth-order architectural units: the extensively connected body unit sandwiched with intermittent channels, the composite channel unit formed by overlapping and separated stable channels, the lateral alternated unit with braided channel and sheet flow sediment, and the runoff channel inlaid in flood plain mudstone.

Based on the theory of high-resolution sequence stratigraphy [19], we established the sequence stratigraphy framework in this study area. We divided 1 long-term, 7 medium-term, and 24 short-term base-level cycles in the target stratum. The time span of the medium and short-term cycles is approximately 0.23 and 0.07 Ma, respectively. The vertical assemblage of different sedimentary microfacies constitutes the sedimentary sequence of the alluvial fan. Its sediments show an upward-fining grain-size distribution, which suggests that the sedimentary sequence is a retrogradation sequence. The physical properties of the reservoir structures include low porosity and ultra-low permeability, and they have average porosity and permeability values of 10.5% and 7.8 mD, respectively.

3. Data and Methods

The reservoir data in the Qie12 area contain various data types: geology, wireline logging, seismic, and production dynamic. The area houses 13 coring wells, including 3 systematic coring wells, and the total core length of the target layer is 309 m. After more than 1000 analyses, the resulting test data, including microreservoir analysis, reservoir sensitivity, and microseepage test, are corrected using core and ground gamma data. These data are detailed and reliable, and they provide data support for the microheterogeneity evaluation of reservoirs. All 127 wells are well-logged, and logging interpretation was performed on these wells. By evaluating the four properties of the reservoir, we established the identification charts of effective reservoirs and interlayers, interpreted and divided the effective reservoirs and interlayers, and clarified the structures of effective reservoirs and distribution styles of interlayers. The three-dimensional seismic work area is approximately 100 km^2. The quality of seismic data obtained at main frequency, frequency band range, and sampling rate values of 30 Hz, 10–50 Hz, and 2 ms, respectively, is good. The research area has been in development and has rich production dynamic data. Its geology, wireline

logging, seismic data, and dynamic production data provided a basis for our reservoir macroheterogeneity evaluation.

There are various methods to evaluate reservoir heterogeneity [20–24]. In this study, we used geological origin, geostatistics, logging interpretation, and analysis of production performance to evaluate the macroheterogeneity of the studied reservoir. Additionally, an experimental method was used to analyze the microheterogeneity of the reservoir. The geological origin affecting reservoir heterogeneity was studied initially using a geological origin method, and the results revealed the main factors that influence heterogeneity and depicted the strength of reservoir heterogeneity. We found that sedimentary factors are the main geological causes of reservoir heterogeneity. Different configuration units of alluvial fans directly determined the strength of macroheterogeneity. Geostatistics is a widely used method for studying reservoir heterogeneity, and this method uses statistical analysis of reservoir permeability to judge the strength of reservoir heterogeneity. It also includes the statistical analysis of the thicknesses and frequencies of reservoir interlayers and the scales and distributions of effective reservoir sand bodies. Meanwhile, the logging interpretation method provides continuous reservoir permeability data through elaborate logging interpretation. The method provides effective reservoir and interlayer identification charts with four-property evaluation, interpretation of effective reservoirs and interlayers on a single well, development positions of interlayers and intralayers, and qualitative description of macroheterogeneity. Continuous reservoir permeability data are also basic data for geostatistics. An analysis of production performance provides a verifiable and effective way to determine reservoir heterogeneity using various dynamic data that directly reflect the strength of reservoir heterogeneity. Experimental analysis is an important tool for studying microheterogeneity. The dynamic conditions of alluvial fans are complex. The lithofacies are diverse, and the microheterogeneity of reservoirs is strong. Thus, with the help of different experimental analysis methods, the following can be achieved: characteristics of the pore structure of the reservoir, insights into the microseepage mechanism of the reservoir, and sensitivity characteristics of the reservoir. These achievements will provide a geological basis for reservoir reconstruction, remaining oil potential tapping, and reservoir management.

4. Results

4.1. Reservoir Microheterogeneity

In this study area, reservoir petrology is characterized by low compositional and structural maturity. The compositional maturity index (Q/(F + R)) is 0.23. The reservoir is poorly sorted, and the main contact method among its particles is the line–point contact relationship. The average mass fraction of its mud base is approximately 8.4%, and its average cement content of 2.1% is relatively low. We utilized various experimental techniques, including thin-section observation, scanning electron microscopy (SEM), mercury injection, and computed tomography (CT) scanning, and their results confirmed the dual porosity media characteristics of the space-type sandy conglomerates in this study area [25,26]. Four types of pores were found in the reservoir: primary intergranular (Figure 3a–d), intragranular dissolution (Figure 3h–j), diagenetic fracture (Figure 3e–g) [27], and argillaceous micropores (Figure 3k,l), and the proportion of primary intergranular pores is >60%. In this study, the diagenesis affecting the sand conglomerate reservoir includes compaction, cementation, and dissolution [28]. Compaction is the main diagenesis to reduce the primary intergranular pores, the average compaction pore reduction and compaction pore reduction rates are 19% and 53%, respectively. The compaction intensity is medium. Additionally, the diagenetic fractures developed due to compaction increased the reservoir pore space and partially improved the reservoir's permeability; this had a certain constructive effect on the reservoir transformation. Cementation is another important factor contributing to the reduction of the primary intergranular pores, with a pore reduction of 3% and a pore reduction rate of 8%. Calcite, anhydrite, and dolomite are mostly distributed in porphyry pores; moreover, they are only partially enriched in the unconformity surface between

the sand conglomerate and the basement rock. Dissolution plays a constructive role in modifying reservoir performance. In this study, dissolution either selectively dissolved feldspar and igneous rock debris to form intragranular pores or spread along diagenetic fractures to create dissolution pores. The dissolution pore enhancement and dissolution pore enhancement rates are 2% and 5%, respectively.

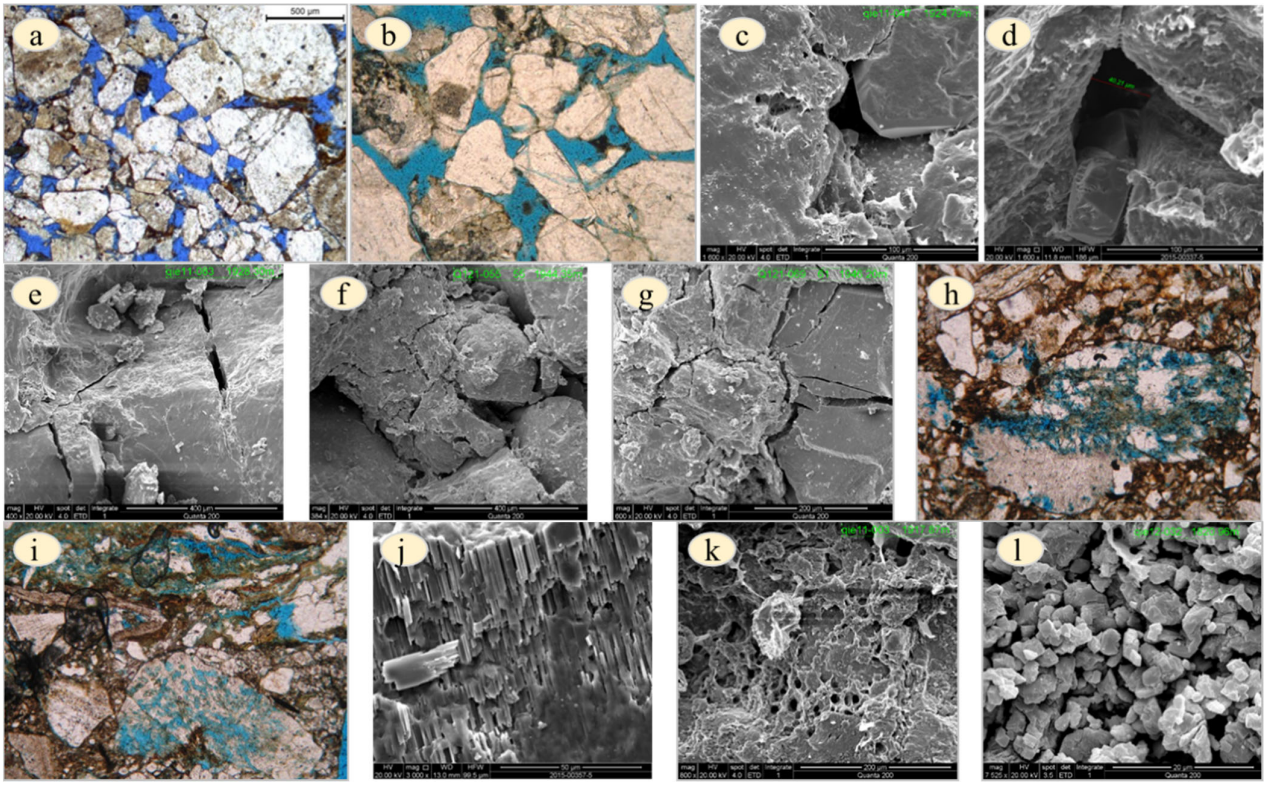

Figure 3. Characteristics of reservoir storage space in the Qie12 block: (**a**) Well Qie12−10−8, 1857.01 m, medium-coarse-grained feldspar lithic sandstone, primary intergranular pores; (**b**) Well Qie11, 1920.13 m, gravel-bearing coarse sandstone, primary intergranular pores, (-) × 25; (**c**) Well Qie11, 1924.79 m, sandy conglomerate, primary intergranular pores; (**d**) Well Qie12−10−8, 1850.82 m, gravel-bearing coarse sandstone, primary intergranular pores; (**e**) Well Qie11, 1928.3 m, sandy conglomerate, cracked fracture; (**f**) Well Qie121, 1944.36 m, cracked fracture; (**g**) Well Qie121, 1946.2 m, cracked fracture; (**h**) Well Qie12, 1818.6 m, gravel-bearing sandstone, detritus dissolution pores, (-) × 25; (**i**) Well Qie12, 1820.5 m, pebbly sandstone, feldspar dissolution pores, (-) × 25; (**j**) Well Q12−7−28, 1831.72 m, sandy conglomerate, feldspar dissolves along the joint; (**k**) Well Qie11, 1917.87 m, sandy conglomerate, argillaceous micropores; and (**l**) Well Qie12, 1820.96 m, argillaceous micropores.

The microheterogeneity of the reservoir is mainly due to various pore structures, which are formed by different sedimentary fabrics [29,30]. Under the same geological background and identical dynamic diagenetic conditions within the reservoir, the grain sizes and cement contents of different sedimentary microfacies are the same. The mud content is the most intuitive reflection that describes the differences in control sedimentary fabrics found in various facies belts of alluvial fans. The high or low contents of the mud controlled the pore structure of the reservoir, and it also determines the strength of the reservoir's microheterogeneity. SEM images of thin sections and particle size data showed two types of pore structures in the reservoir of this study area; furthermore, these structures are bimodal and multimodal.

The bimodal pore structure of the reservoir is supported by gravel, forming a skeleton that is filled with sandy debris. Alternatively, the gravel is suspended in the sandy debris,

the grain-size histogram is bimodal, and the main grain-size interval is fine gravel and giant sand–fine sand with low clay content (Figure 4a,b). The reservoir space is characterized by combinations of primary intergranular pores, intergranular dissolved pores, and diagenetic fractures. The proportion of primary intergranular pores is >70%, and the pores observed in thin sections are well developed. We performed two experimental analyses, namely conventional and constant-rate mercury intrusions, to characterize the pore structure of the reservoir. The conventional method mainly reflects the change in the pore volume during mercury intrusion, while the constant-rate method highlights the number distribution of pores and throat tracts. In pore structure analysis and statistics, the quantity distribution is more accurate than the volume distribution, particularly the quantity distribution of the throat tract, which can better characterize the reservoir's seepage characteristics. The results of mercury intrusion experiments revealed pore structures in the reservoir of coarse skewness, well sorted, low drainage pressure, and median pressure. Macropores and mesopores are the dominant pore sizes, and their main peak value is approximately 125 μm, which suggests a unimodal distribution. The distribution of throats, which are mainly fine throats, is not significant, and the radii of the mainstream throats are in the range of 3.05–10.22 μm. Local large throats are also found, and the average pore–throat ratios obtained for the reservoir are in the range of 58.51–130.94. CT scanning revealed that the percentage of pore–throat volume is 52%. This modal type is developed in most braided channel microfacies and the minority of runoff channel microfacies that are effective reservoirs.

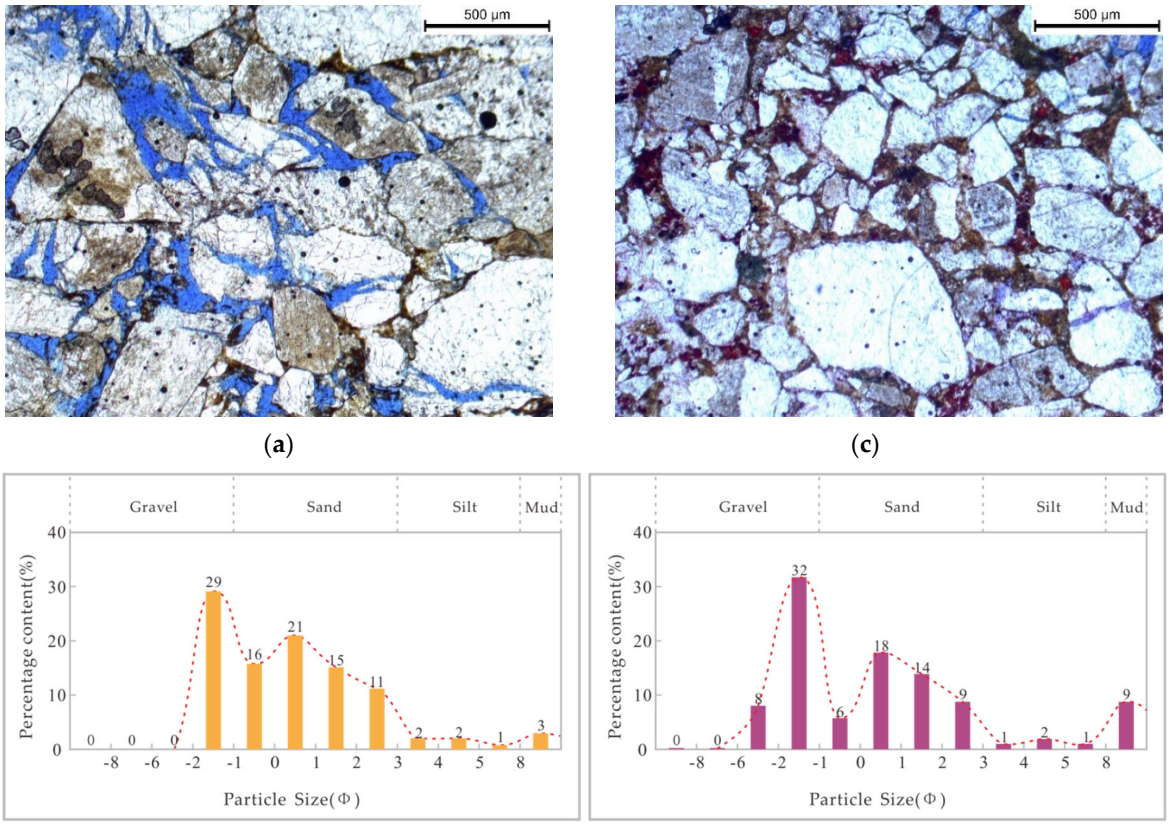

Figure 4. A chart of the reservoir structure model for the Qie12 block: (**a**) Well Qie12−10−8, 1858.06 m, gravel-bearing medium-coarse feldspar sandstone, primary intergranular pores; (**b**) Well Qie12−10−8, 1858.06 m, histogram of particle size distribution; (**c**) Well Qie12−10−8, 1859.4 m, argillaceous sandy conglomerate, dissolution pores, and argillaceous pores are the main pore types, rarely with visible pores; and (**d**) Well Qie12−10−8, 1859.4 m, histogram of particle size distribution.

The multimodal pore structure of the reservoir is complex, and it is composed of gravel, sand, and clay. The clay content is high, and the histogram of the grain size distribution shows multiple peaks (Figure 4c,d). The reservoir space is characterized by a combination of intergranular dissolved pores and argillaceous micropores. Although the primary intergranular pores under thin sections are poorly developed, they seem to be filled mostly with argillaceous interstitial fillers. The pore structures of the reservoir are characterized by fine skewness, poorly sorted, high displacement pressure, pore–throat distribution, multi-peak forms, and small pore–throat radius. This mode type is mainly developed in debris flow, diffuse deposition, and the majority of runoff channel microfacies, and it is manifested in poor reservoir and nonreservoir.

4.2. Reservoir Macroheterogeneity

Reservoir macroheterogeneity is controlled primarily by the spatial and temporal distribution of different sedimentary configuration units of the alluvial fan. This heterogeneity determines the depositional architecture, rhythm, geometry, and connection mode of sand bodies of different origins; thus, it directly affects the characteristics and strength of macroheterogeneity [31,32].

4.2.1. In-Layer Heterogeneity

In-layer heterogeneity refers to the variation rule of vertical reservoir parameters in small layers (e.g., rhythmic characteristics of vertical permeability, interlayer types, and distribution styles) [33,34], and it is a key geological factor controlling the swept volume of vertical injectors and the remaining oil distribution in small layers.

Characteristics of Rhythms

Based on the data obtained from the core physical property analysis, the permeability rhythmic characteristics of the single sand body in this study area have two rhythm types: compound and homogeneous. The former is a typical characteristic of the sand body in the braided channel. The median grain size of sands in the sand body shows positive and compound positive rhythms, and the wellbore logging curve characteristics show bell and box shapes. WellQ11, with a depth range of 1929–1932 m, has a typical permeability compound rhythm that is composed of a single-granularity positive rhythm (Figure 5a). The bottom of a rhythm is controlled by hydrodynamic conditions, and it has coarse grains that are mainly composed of gravel with poorly sorted sedimentary fabric and poor permeability. In the middle section of the rhythm, the hydrodynamic energy is moderate, and the sand is mainly coarse-medium in grain size and well-sorted with low mud content and good permeability. In the upper section of the rhythm, the channel energy is attenuated, which turns the grain sizes to fine (mainly fine-silty sand), and the fabric sorting is medium. The mud content in this section is high, and its permeability is poor. Its permeability rush coefficient and ratio are 3.3 and 126, respectively. Finally, this section has strong heterogeneity.

WellQ11, with a depth range of 1923.0–1926.5 m, has a composite permeability rhythm composed of two or more single-granularity positive rhythms that are superposed on top of each other (Figure 5b). It is formed by aqueduct accretion, and it has strong heterogeneity. The change in its permeability in the longitudinal direction is very complicated. Its permeability rush coefficient and ratio are 3.6 and 175, respectively. The primary rhythm type in its sheet flow and debris flow sand body is homogeneous. It has poor fabric sorting, mixed base support, massive structure, and no obvious grain rhythm. Its reservoir permeability is poor, but the reservoir is relatively homogeneous.

WellQ12-10-8, with a depth range of 1872–1875 m, is a homogeneous rhythmic debris flow deposit (Figure 5c). Its permeability rush coefficient and ratio are 1.7 and 18, respectively.

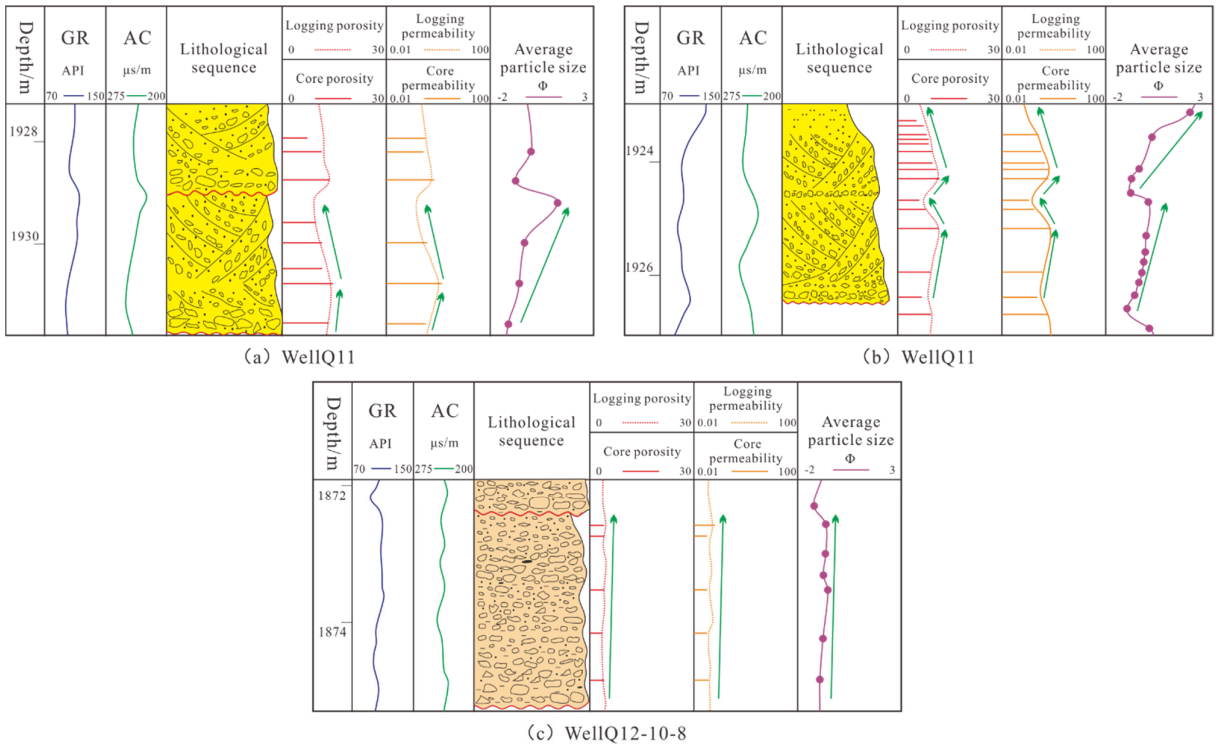

Figure 5. Rhythm characteristics of the Qie12 block in the Kunbei oilfield: (**a**) Well Qie11, 1929–1932 m, single-granularity positive rhythm; (**b**) Well Qie11, 1923.0–1926.5 m, composite permeability rhythm; (**c**) Well Qie12−10−8, 1872–1875 m, homogeneous rhythm.

Quantitative Evaluation of the Range of Permeability Difference

Quantitative evaluation of the intralayer permeability difference in this study area includes the following parameters: average permeability, permeability ratio, and permeability rush coefficient. The distribution histograms of permeability difference and permeability rush coefficient are shown in Figure 6. For IV-6 and IV-7 layers, the permeability difference, rush coefficient, and average permeability ranges are 33–43, 2.5–2.7, and 0.10–1.56 mD, respectively. These values reflect the lack of a high-permeability braided channel reservoir in the extensively connected body unit sandwiched with intermittent channels of the inner fan. They also suggest poor reservoir storage performance and medium heterogeneity. For IV-4 and IV-5 single layers, the permeability difference, rush coefficient, and mean permeability ranges are 72–74, 3.8–4.1, and 4.71–25.41 mD, respectively. These values suggest good reservoir performance in the composite channel unit formed by overlapping and separated stable channels in the alluvial fan. This unit has a high-permeability section that intensifies reservoir heterogeneity, and it is the most heterogeneous configuration unit in the alluvial fan. The IV-3 single layer has values for permeability difference, rush coefficient, and average permeability of 45, 3.3, and 3.2 mD, respectively. These values reflect poor reservoir performance and low heterogeneity in the lateral alternated unit with braided channel and sheet flow sediment of the middle fan; however, the overall heterogeneity is still high. In the IV-1 and IV-2 single layers, mudstone in their flood plain is regional cap rock, and the reservoir is poorly developed.

In-Layer Type and Distribution Style

Systematic coring wells reveal the absence of mudstone interlayers in the thick sandy conglomerate section. However, the characteristics of the oil-bearing sections, oil infiltration, oil spot, and oil trace, are discontinuous, showing the interbedded distribution of these sections and the oil-free section. On the basis of the oil test results, the oil-free section is not a water layer. The main reason for the vertical difference in oil content is the presence of muddy interlayers and part of partial calcareous interlayers, which are controlled by the

different sedimentary fabrics or cements. The pore structure of the muddy interlayer is multimodal. This interlayer has a high content of clay mineral matrix and tight physical characteristics. The wellbore logging curve suggests the following features: high natural gamma-ray, high acoustic time, low resistivity, high nuclear magnetic total porosity, and mainly argillaceous micropores. The pore structure of the calcareous interlayers is also multimodal. These interlayers have high cement carbonate content and medium clay mineral matrix. In contrast to the muddy interlayer, the wellbore logging curve of a calcareous interlayer suggests the following features: low natural gamma-ray, low acoustic time, high resistivity, and low nuclear magnetic total porosity. We determined the lower limit of physical property, the upper limit of muddy content, and the logging curve parameters of the effective reservoir and interlayer using a four-property relation analysis. These enabled us to establish the quantitative identification plate (Table 2) of the effective reservoir and interlayer.

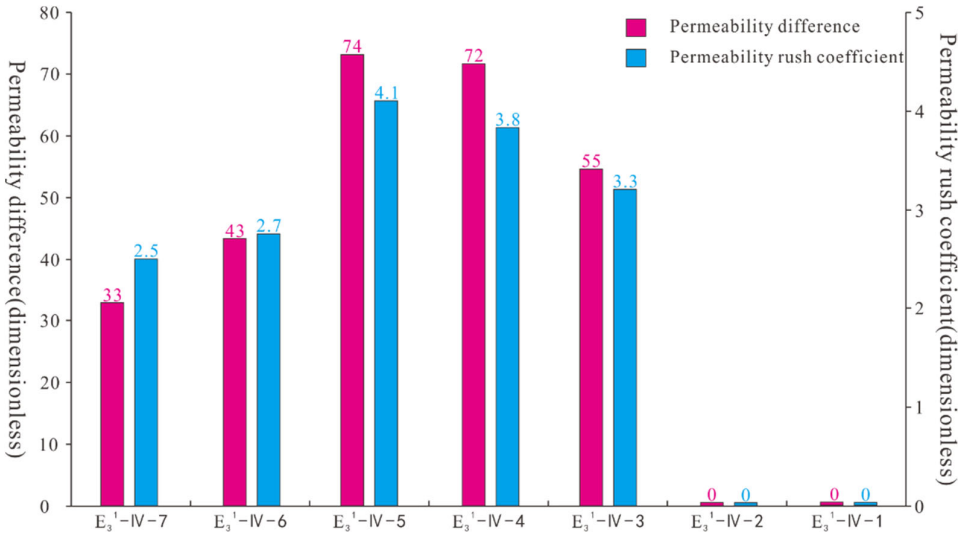

Figure 6. Distribution histograms of permeability difference and permeability rush coefficient.

Table 2. Identification plate of effective reservoir and interlayer in the Qie12 block.

Type	Permeability (mD)	Porosity (%)	Shale Content (%)	AC (μs·m^{-1})	ΔGR	LLD (Ω·m)	Sedimentary Facies
Effective reservoir	>0.6	>8.5	<5	>230	<0.55	>8	Braided channel
Muddy interlayer	<0.6	<8.5	>8	>230	>0.55	5–8	Debris flow/sheet flow/abandoned channel/silted channel deposit/runoff channel
Calcareous interlayer	<0.6	<8.5	5–8	<230	<0.6	>8	Riverbed detention deposit of braided channel/runoff channel/glutenite above the unconformity surface

The identification and division of effective reservoir and interlayer are performed for all wells using the quantitative identification plates. After comparing the effective reservoir and interlayer, we conclude the presence of two interlayer distribution patterns: (1) layer-cake architecture and (2) generally scattered and locally interlaced (Figure 7). The former pattern is formed primarily at the extensively connected body unit sandwiched with intermittent channels of the inner fan. This pattern is laminar with stacked interlayers that divide the lenticular effective reservoir sand body, and its seepage barrier has the strongest shading capacity among all the alluvial fan architectural units. The latter pattern develops in the composite channel unit formed by overlapping and separated stable channels and the lateral alternated unit with braided channel and sheet flow sediment of the middle

fan. It is manifested as partial discontinuities in the grid of "plywood" high-permeability reservoirs. As the channels gradually shrink and die out, the pattern's sheet flood deposits increase, and the scale of its interlayer development increases gradually.

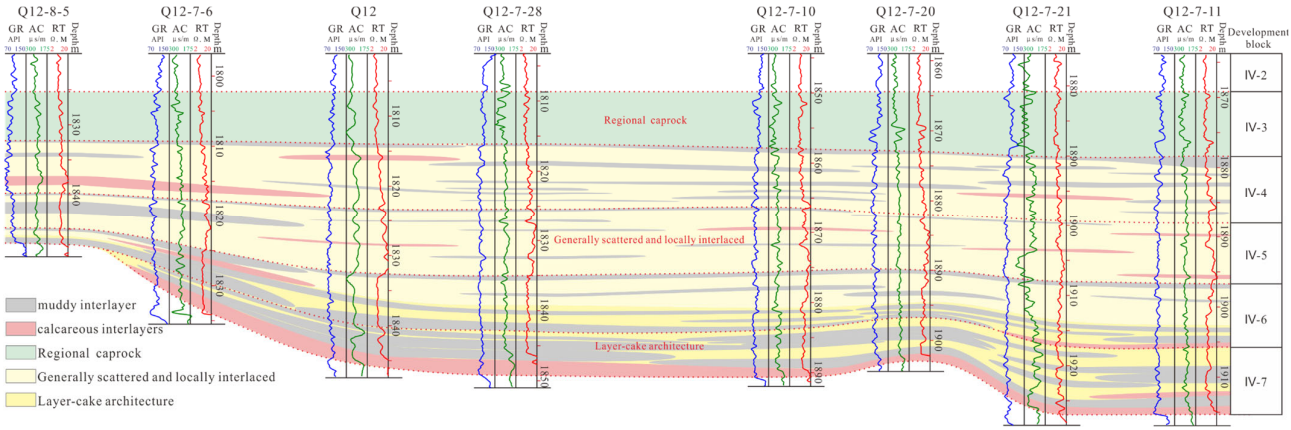

Figure 7. The interlayer distribution of the Qie12 block.

The isolation ability of an interlayer mainly depends on its permeability, which increases variably with increasing interlayer thickness. Parameters such as thickness, density, and frequency are often used to quantitate the distribution pattern of an interlayer [35]. On the basis of our measurements, the thickness and density of the interlayer in this study area from bottom to the top showed a characteristic change from large to small and then to large, whereas its frequency increased gradually. The highest and lowest density values are found in layers IV-7 (0.78%) and IV-5 (0.38%), respectively. Meanwhile, the highest and lowest frequency values are found in layers IV-3 (0.23 bars/m) and IV-7 (0.09 bars/m), respectively.

4.2.2. Interlayer Heterogeneity

Interlayer heterogeneity, which refers to the differences between sand bodies, including cyclicity of strata system, distribution of sand barrier, and characteristics of interlayer fractures, is an important cause of interlayer interference and water displacement differences during water injection development. We focused on the characteristics of interlayer barriers and found that barriers between layer IV-7 and its overlying basement rock are the most developed. These 1.1–2.8-m-thick barriers showed a stable lateral distribution and good continuity. The barriers between layers IV-6 and IV-7 have a more continuous lateral distribution, and their thickness is in the range of 0.5–2.3 m. The barriers between layers IV-5 and IV-6 and layers IV-3 and IV-4 have a discontinuous lateral distribution, and their thickness in the range of 0.4–1.6 m is small. Meanwhile, the barriers between layers IV-4 and IV-5 are developed on a small scale, and their thickness is in the range of 0.3–0.5 m. They are also poorly continuous, and their isolation ability is limited. The development scale and distribution pattern of the interval layers are controlled by the architectural unit type; thus, serious heterogeneity in the development of water injection is present in different architectural units, which limits the effectiveness of reservoir waterflood.

4.2.3. Horizontal Heterogeneity

Reservoir horizontal heterogeneity is caused by the geometry, scale, and continuity of the sand body and its permeability planar variation. It directly affects the waterflood-swept area and planar water displacement efficiency.

Sand Body Geometry

Sedimentary facies determine the geometry of sand body distribution. The 5.8–62.0-m-thick alluvial fan sandy conglomerate in this study area is distributed with a thin western to thick eastern distribution. Controlled by the development scale of the braided channels

in different sedimentary architectural units, the effective sand body developed two types of reservoir architecture. One is jigsaw-puzzle reservoir architecture, which developed in the composite channel unit formed by overlapping and separated stable channels of the middle fan. The plane geometry is fan-shaped, but with the channel shrinkage, the plane geometry becomes dendritic. The other is the labyrinth architecture, which is developed in the extensively connected body unit sandwiched with intermittent channels. The lenticular effective sand body is distributed sporadically, and its geometric shape is similar to a potato.

Sand Body Connectivity

Through a good correlation comparison of effective sand bodies with interlayers in this study area, we concluded the presence of four sand body connectivity mode types: disconnected, weakly connected, connected multilayer, and connected multilateral type, which are shown in Figure 8a–d, respectively. The disconnected, weakly connected, and two-connected types account for 20%, 35%, and 45% of the total, respectively. The disconnected type mainly develops in the extensively connected body unit sandwiched with intermittent channels. The weakly connected type develops mainly in the lateral alternated unit with braided channel and sheet flow sediment. Meanwhile, the connected types mainly develop in the composite channel unit formed by overlapping and separated stable channels, and they play an important role in controlling water injection and well pattern arrangement.

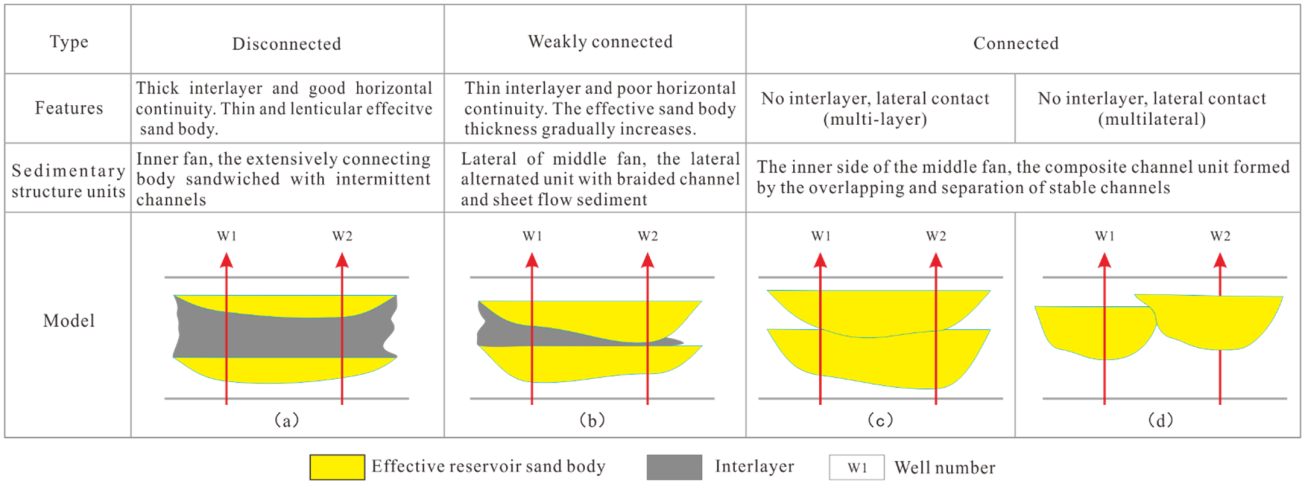

Figure 8. Sand body connecting type of the Qie12 block: (**a**) disconnected; (**b**) weakly connected; (**c**) connected multilayer; (**d**) connected multilateral.

Distribution of Reservoir Permeability and Permeability Variation Coefficient

We analyzed the horizontal distribution characteristics of reservoir parameters using a geostatistics method with E_3^1-IV-4 as an example. The average permeability, mean variation coefficient, mean range difference, and rush coefficient of the selected single reservoir are 7.8 mD, 0.86, 66.3, and 3.4, respectively. A comprehensive evaluation of reservoir heterogeneity is strong. The permeability distribution map of the reservoir is shown in Figure 9a. The long axis of the isoline is in the direction of northwest to southeast. The permeability changes from low to high and then to low from west to east, and the composite channel in the middle fan has the best permeability. The permeability variation coefficient is distributed in a circular band, as shown in Figure 9b. The composite channel unit heterogeneity in the inner side of the middle fan is the strongest, and its variation coefficient is >0.7. This unit is followed by the lateral alternated unit with braided channel and sheet flow sediment on the lateral side of the middle fan, and its variation coefficients are in the range of 0.3–0.9. The extensively connected body unit sandwiched with intermittent channels in the inner fan showed moderate reservoir heterogeneity, with its variation coefficients in the range of 0.3–0.5.

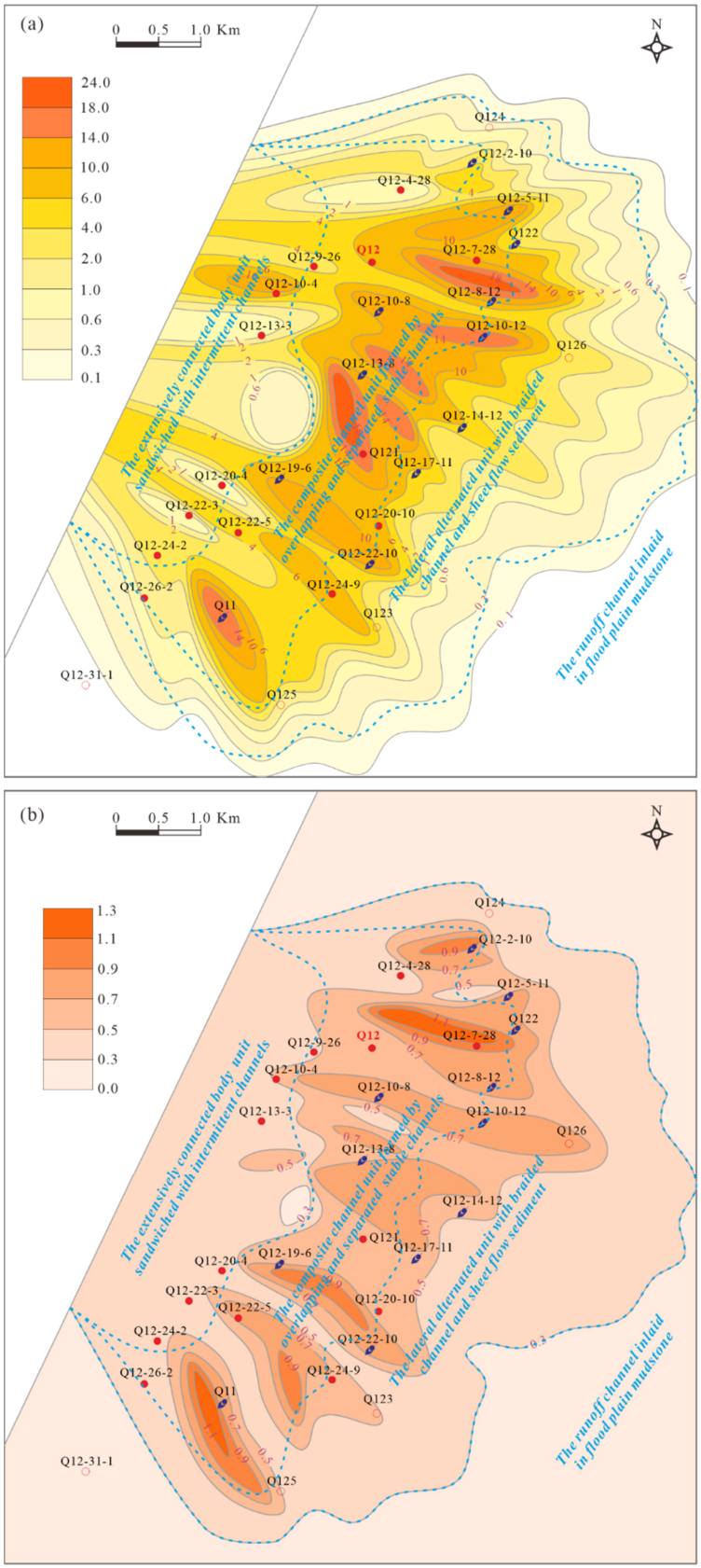

Figure 9. (**a**) Permeability and (**b**) variation coefficient distribution of the E31-IV-4 formation in the Qie12 block.

5. Discussion

Reservoir heterogeneity from macroscopic to microscopic and from intralayer to interlayer and plane is the main factor that controls the distribution of remaining oil [36–38]. Thus, the geological factors that control the distribution of the remaining oil in alluvial fan glutenite reservoirs include the distribution pattern of flow barriers, permeability rhythm characteristics, and reservoir microscopic pore structure of the sedimentary architectural unit.

5.1. Influence of Flow Barrier Pattern on Remaining Oil Distribution in Architectural Units

The hydrocarbon distribution in this study area is uneven and segmented according to the description of the systematic coring of Well Q12-10-8. There are four oil segments from bottom to top. The segment at the bottom contains the least oil and a significant amount of massive barren argillaceous conglomerates. The middle segment contains a relatively continuous oil distribution segment, which is regarded as the best oil-bearing interval in the alluvial fan. This segment is mainly composed of oil-immersion, oil-bearing, and oil-patch sandy conglomerates or pebbly coarse-medium sandstones. It also contains thin barren muddy glutenite. The upper segment has a discontinuous property of oiliness and is composed of oil-patch and oil-immersion sandy conglomerates, pebbly sandstone, barren muddy glutenite, and anisometric sandstone. The topmost segment is barren, and it contains massive mudstones that do not have oil and gas.

After analyzing the relationship between hydrocarbon enrichment characteristics and the liquid production profile of architectural units, we found that the effective reservoir architecture and flow barrier distribution pattern of different architectural units control the vertical "four-segmentation" enrichment law of hydrocarbon and affect the macroscopic distribution of remaining oil (Figure 10).

In the extensively connected body unit sandwiched with intermittent channels, the effective reservoir with a lenticular shape distribution is isolated by "layer-cake architecture" interlayers, resulting in poor oiliness properties. The reservoir has poor permeability and injection–production connectivity, and it has a high starting water pressure that slows waterline advancement. It manifests as under-injection or no injection and has a relative water absorption of <20%. It has poor sweep efficiency of injected water and degree of water driving and produces flake-like remaining oil.

In the composite channel unit formed by overlapping and separated stable channels, some interlayers have a "generally scattered and locally interlaced" distribution in the unit's effective reservoir, having a plate-like synthesis distribution. Therefore, the best oiliness property and most continuous hydrocarbon distribution are found in the proximal part of the middle fan. The injection–production connectivity rate, sweeping efficiency of water injection, and degree of water driving in this unit are high. A total of 90% of daily oil production and 80% of relative water absorption occur in this unit. In the lateral alternated unit with braided channel and sheet flow sediment, there is gradual shrinkage of the braided channel and a gradual increase of sheet flow sediments. In addition, the thickness of the effective reservoir reduces, whereas the thickness and the frequency of interlayers increase. Meanwhile, hydrocarbon distribution becomes discontinuous in the distal part of the middle fan, and both liquid production and water absorption significantly decrease. In the aforementioned two units, according to the perforation plan of "large diameter casing pipe and mixed injection," the injected water passes quickly along large channels in the high-permeability reservoir, resulting in water flooding, and the unswept area of injected water forms plaque-like remaining oil.

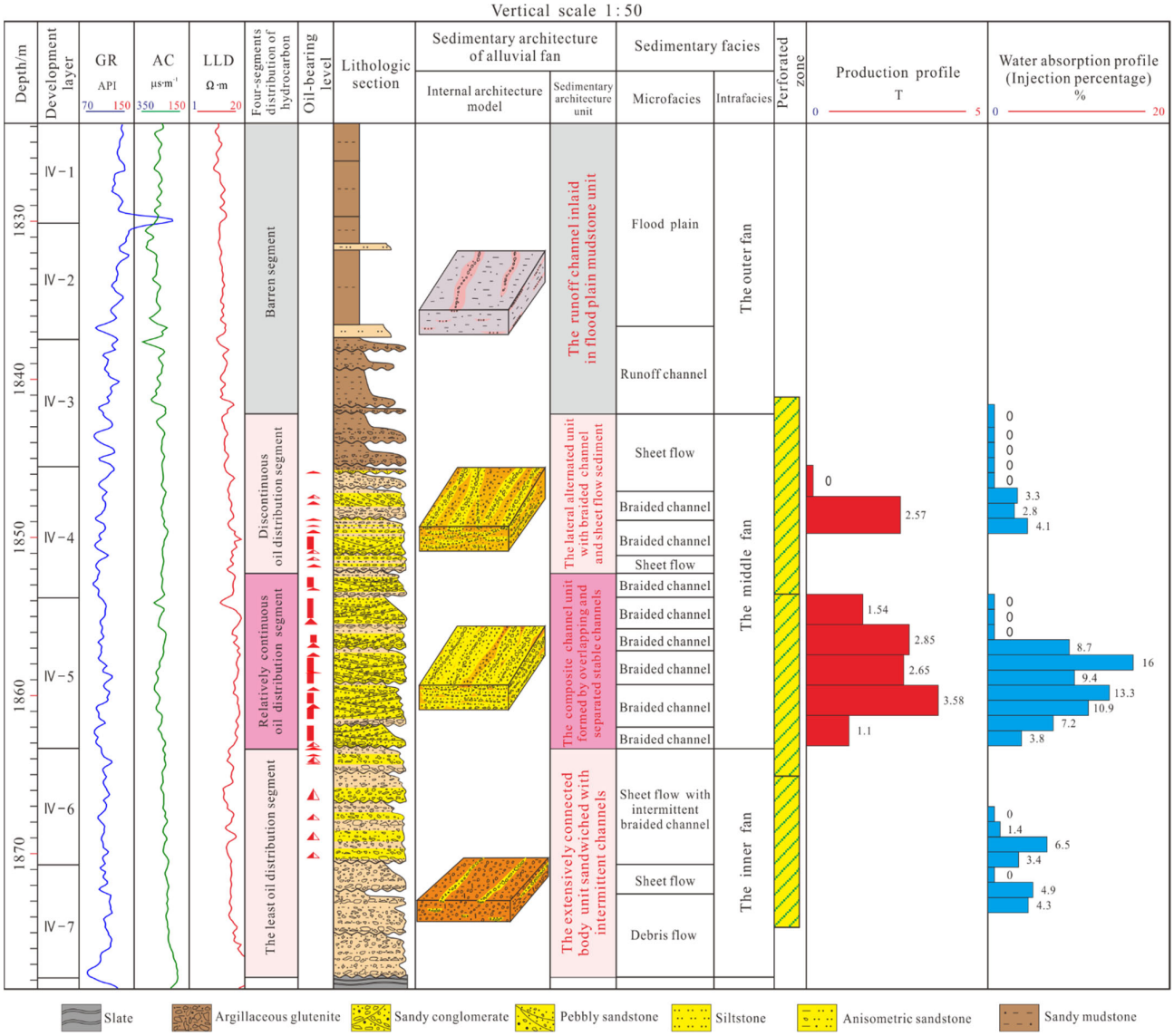

Figure 10. Relationship between production profile and sedimentary architectural units.

5.2. Influence of Permeability Rhythm on Macroscopic Remaining Oil Distribution

The water absorption profile of the 1922- to 1935-m braided channel sand body in Well Qie11 is shown in Figure 11. We used this profile as an example to analyze the influence of reservoir permeability rhythm characteristics on the macroscopic remaining oil distribution. There are four permeability composite rhythms developed vertically in this section reservoir. In the middle and lower parts of the rhythm, the injected water flows easily along the large pores of the high-permeability layer because of the superposition of gravity and intralayer heterogeneity effects. Relative water absorption accounts for approximately 85% of the reservoir's total in Well Qie11 water absorption profile. After the water injection front breaks through, the water cut of the production well rises rapidly, and the injected water circulates ineffectively. In the upper part of the rhythm layer, the water breakthrough flow is slow, relative water absorption accounts for approximately 15%, oil displacement efficiency is low, and the remaining oil is enriched.

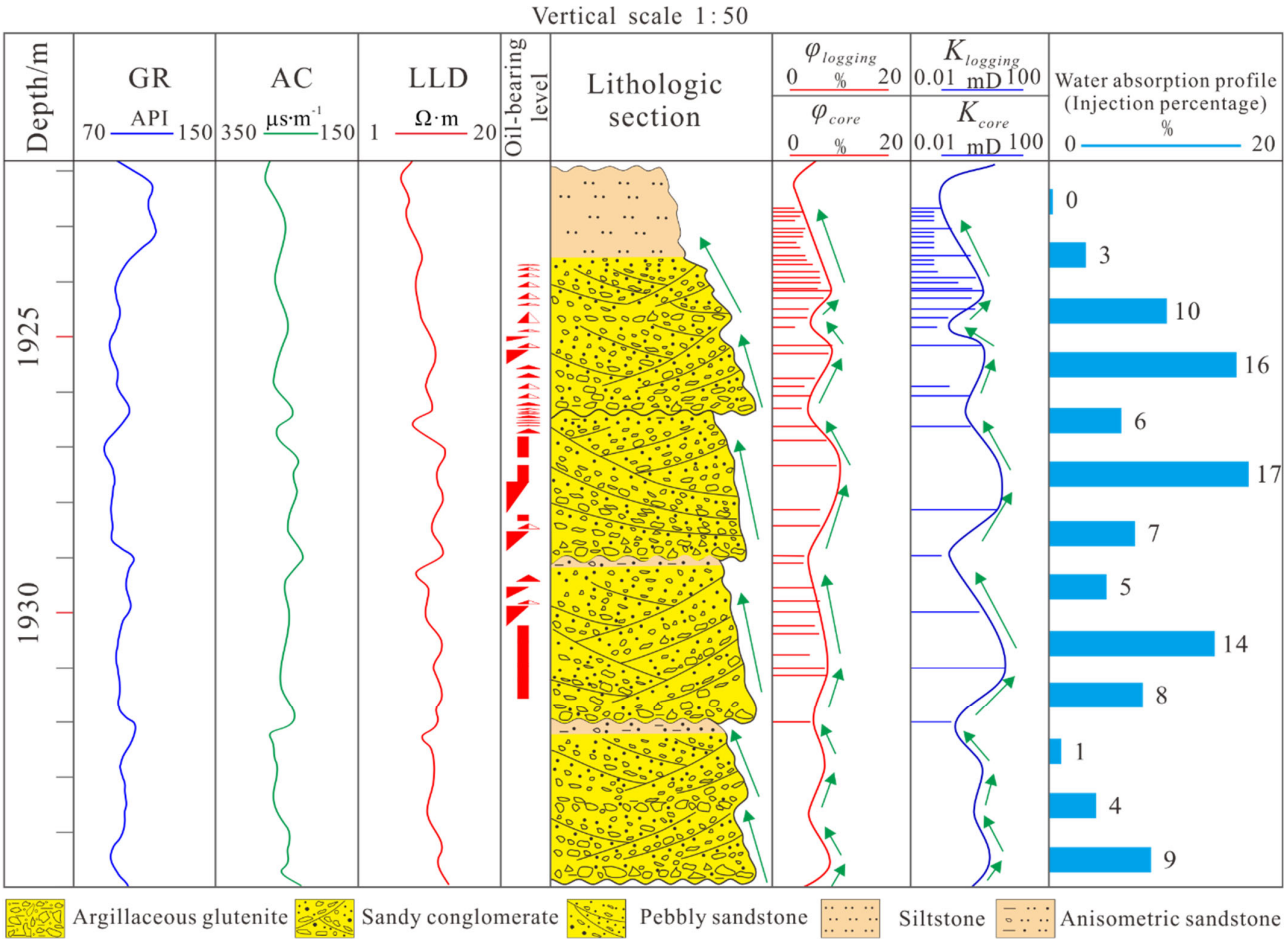

Figure 11. Relationship between permeability compound rhythmicity and water absorption.

5.3. Influence of Reservoir Microheterogeneity on Microscopic Remaining Oil Distribution

The flow in the large pores of the bimodal reservoir pore structure is the main factor that leads to the strong heterogeneity of microscopic seepage [39,40]. The microscopic flow experiment shows the following results: the water displacement process is characterized by heterogeneous flooding, the water-free oil recovery period is short, and oil displacement efficiency is relatively low. In the process of water displacement, the heterogeneous intrusion and flow around the water flooding front form a large area of remaining oil that is not displaced by the surrounding flow and island-shaped remaining oil, as shown in Figure 12a,b, respectively. Water phase permeability is low in the presence of remaining oil; thus, the injected water is more likely to penetrate along the pore channels that have been broken through. Therefore, it is difficult to displace oil with the injected water, resulting in low oil displacement efficiency and a rapid increase in water content.

In summary, reservoir heterogeneity plays an important role in controlling the distribution of remaining oil. We note that deep profile control and oil displacement technique are key to the comprehensive management of the composite channel unit formed by overlapping and separated stable channels or the lateral alternated unit with braided channel and sheet flow sediment. Meanwhile, to tap the potential of the remaining oil in the extensively connected body unit sandwiched with intermittent channels, we need to depressurize, increase the injection, and improve the quality of the reservoir. The study effectively guided the deep profile control of the test well group, and it achieved practical results. Under the premise of an unchanged production system and after profile control, the daily fluid production of a single test well (i.e., Q12H13-9) was stable (Figure 13). The test well's daily oil production increased by approximately 40%, whereas its water content decreased by 35%.

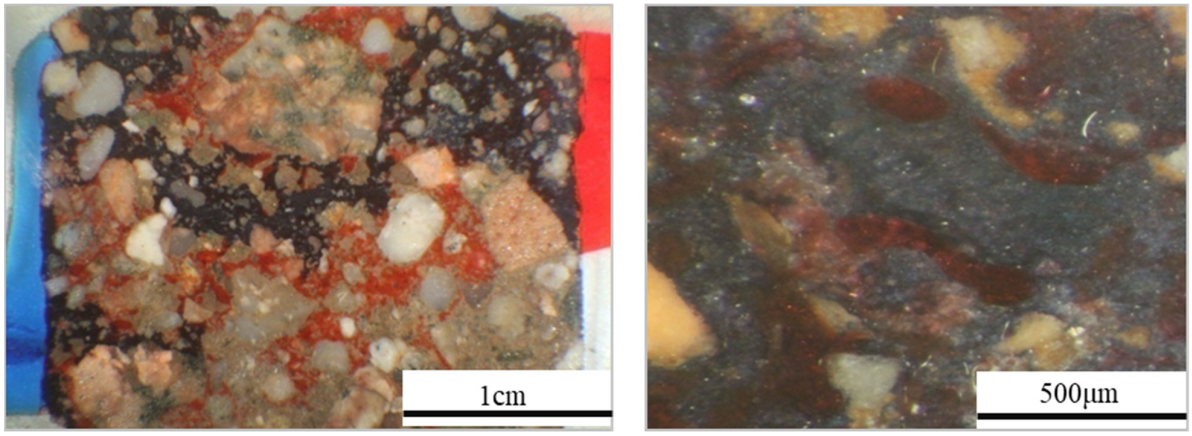

Figure 12. Distribution model of the remaining oil in the Qie12 block. (**a**) Surrounding flow remaining oil, Well Qie12−7−8, 1814.92 m; (**b**) island-shaped remaining oil, Well Qie12−7−28, 1844.12 m.

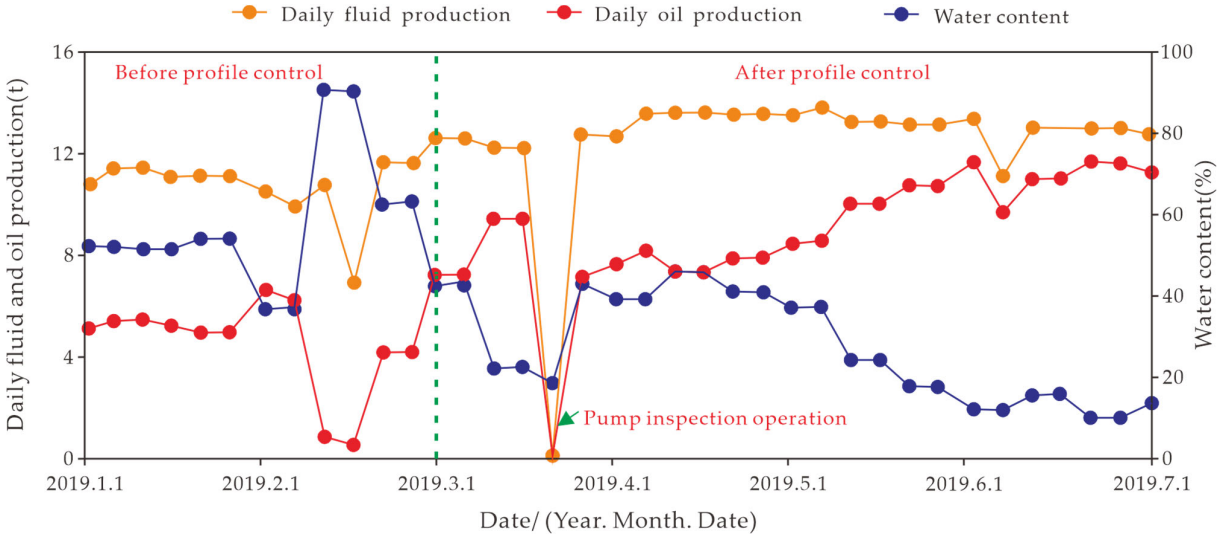

Figure 13. Oil production rate curve of the Q12H13−9 well in the Qie12 block.

6. Conclusions

The results of this study showed that the alluvial fan reservoir exhibited strong heterogeneity. By considering sedimentary architectural units as the research object, we qualitatively and quantitatively investigated the microheterogeneity and macroheterogeneity of a sandy conglomerate reservoir. Based on these results, we discussed the effect of heterogeneity on the remaining oil distribution and highlighted the main measures required to tap the remaining oil in different architectural units.

Note that reservoir heterogeneity is the geological basis of reservoir management. This is the first study to propose the concept based on sedimentary architectural units. These are important for the comprehensive reservoir management in the Qie12 block, but would also be relevant in other alluvial fan reservoirs.

(1) The difference in reservoir pore structures that are controlled by the different sedimentary fabrics is the main cause of reservoir microheterogeneity, whereas the spatial and temporal distribution of alluvial fan sedimentary architecture units is the main factor that controls reservoir macroheterogeneity.

(2) Reservoir heterogeneity affects the distribution of remaining oil through the flow barrier distribution pattern of sedimentary architecture units, permeability rhythm, reservoir pore structure, and other aspects. The remaining oil distribution of different

structural units is different. The composite channel unit formed by overlapping and separated stable channels or the lateral alternated unit with braided channel and sheet flow sediment is affected by the inhomogeneous inching of injected water along the large pore–throat channel. The remaining oil is formed in patchy distributions, such as flow around an island, and it is enriched in the upper part of the composite rhythmic layer. Therefore, deep profile control and oil displacement technologies are keys to the comprehensive management of these units. In the extensively connected body unit sandwiched with intermittent channels, poor injection–production connectivity and low reservoir permeability caused flake-like remaining oil distribution. To fully realize the potential of the remaining oil, the fundamental requirements are depressurization, increase in injection, and improvement of reservoir quality.

(3) The research results have guiding significance for comprehensive reservoir management. Daily oil production increased by approximately 40%, whereas water content decreased by 35%.

Author Contributions: Conceptualization and writing–original draft preparation, Q.G. and C.Z.; writing–review and editing, Y.J.; reservoir microscopic heterogeneity, Z.L. and Q.G.; reservoir macro-heterogeneity, Q.G., B.W. and L.X.; resources, Z.S. and L.X.; data curation, J.W. and Y.J. All authors have read and agreed to the published version of the manuscript.

Funding: This study was financially supported by PetroChina's 14th Five-year Forward-looking Fundamental Scientific and Technology Projects: Research on Reservoir Formation Law and Key Technology of Lithologic Stratigraphic Oil and Gas Reservoirs (2021DJ0402) and Research on Oil and Gas Enrichment Law and Exploration Evaluation Technology in Continental Deep and Ultra-deep Layers (2021DJ0202).

Data Availability Statement: Not applicable.

Acknowledgments: We would like to thank the PetroChina Hangzhou Research Institute of Geology and the PetroChina Qinghai Oilfield Company for permission to release their data. The first author would like to express warm gratitude to all those who supported this research. This paper describes objective technical results and analysis. Comments from anonymous reviewers greatly improved the manuscript.

Conflicts of Interest: The authors declare no conflict of interest.

References

1. Qiu, Y. The methodology of petroleum development geology. *Pet. Explor. Dev.* **1996**, *23*, 43–47.
2. Weber, J.K. Influence of Common Sedimentary Structures on Fluid Flow in Reservoir Models. *Int. J. Rock Mech. Min. Sci. Geomech. Abstr.* **1982**, *34*, 665–672. [CrossRef]
3. Douglas, S.; Hamilton. Approaches to identifying reservoir heterogeneity in barrier/strandplain reservoirs and the opportunities for increased oil recovery: An example from the prolific oil-producing Jackson-Yegua trend, south Texas. *Mar. Pet. Geol.* **1995**, *12*, 273–290.
4. Yang, S. A new method for quantitatively studying reservoir heterogeneity. *J. Univ. Pet.* **2000**, *24*, 53–56.
5. Zhang, W.; Zhang, J.; Xie, J. Research on reservoir bed heterogeneity, interlayers and seal layers and controlling factors of 2+3 sands of upper second member, Shahejie formation, in the west of the Pucheng Oilfield. *Pet. Sci.* **2008**, *21*, 135–144. [CrossRef]
6. Kaviani, D.; Valkò, P.; Jensen, J. Analysis of injection and production data for open and large reservoirs. *Energies* **2011**, *4*, 1950–1972. [CrossRef]
7. Zheng, Z.; Wu, S.; Xu, C.; Yue, D.; Wang, W.; Zhang, F. Lithofacies and reservoirs of allluvial fan in the Lower Keramay formation in the block-6 of Karamay Oilfield, the Junggar Basin. *Oil Gas Geol.* **2010**, *31*, 463–471.
8. Kong, F. Exploration technique and practice of sandy-conglomeratic fans in the northern part of Dongying depression. *Acta Pet. Sin.* **2000**, *21*, 27–31.
9. Lei, Z.; Bian, D.; Du, S.; Wei, Y.; Feng, H. Characteristics of fan forming and oil-gas distribution in west-north margin of Junggar Basin. *Acta Pet. Sin.* **2005**, *26*, 8–12.
10. Simlote, V.N.; Ebanks, W.J.; Eslinger, E.V. Synergistic evaluation of a complex conglomerate reservoir for enhanced oil recovery, barrancas formation, Argentina. *J. Pet. Technol.* **1982**, *37*, 295–305. [CrossRef]
11. Shelby, J.M. Geologic and Economic Significance of the Upper Morrow Chert Conglomerate Reservoir of the Anadarko Basin. *J. Pet. Technol.* **1980**, *32*, 489–495. [CrossRef]

12. Carr, D.L.; Oliver, K.L. Surface-bounded reservoir compartmentalization in the Caddo Conglomerate, Boonsville (Bend Conglomerate) gas field, Fort Worth Basin, Texas. *AAPG Bull.* **1996**, *5*. [CrossRef]
13. Lin, L.; Mu, Z.; Ma, D.; Kou, F.; Jing, H. Characteristics and control factors of the E31 clastic rock reservoir in the Q12 block of the Kunbei oilfield. *Spec. Oil Gas Reserv.* **2011**, *18*, 26–29.
14. Fu, S.; Ma, D.; Wang, L.; Feng, Q.; Xue, J.; Chen, Y.; Zhang, X.; Kou, F. Characteristics and accumulation conditions of paleo-uplift reservoirs in Kunbei thrust belt, Qaidam Basin. *Acta Pet. Sin.* **2013**, *34*, 675–682.
15. Gong, Q.; Shou, J.; Huang, G.; Li, S.; Wang, Y. Sedimentary characteristic of braided delta in Lulehe Formation of Kunbei oilfield in Qaidam Basin. *Chin. J. Geol.* **2012**, *47*, 116–128.
16. Miall, A.D. *The Geology of Fluvial Deposits*; Springer: Berlin/Heidelberg, Germany, 1996; pp. 75–178.
17. Decelles, P.G.; Gray, M.B.; Ridgway, K.D.; Cole, R.B.; Pivnik, D.A.; Pequera, N.; Srivastava, P. Controls on synorogenic alluvial-fan architecture, Beartooth Conglomerate (Paleocene), Wyoming and Montana. *Sedimentology* **1991**, *38*, 567–590. [CrossRef]
18. Wu, S.; Fan, Z.; Xu, C.; Yue, D.; Zheng, Z.; Peng, S.; Wang, W. Internal architecture of alluvial fan in the Triassic Lower Karamay Form ation in Karamay Oilfield, Xinjiang. *J. Paleogeography* **2012**, *14*, 331–340.
19. Cross, T.A. Stratigraphic controls on reservoir attributes in continental strata. *Earth Sci. Front.* **2000**, *7*, 322–350.
20. Yazynina, I.V.; Shelyago, E.V.; Abrosimov, A.A.; Yakushev, V.S. New method of oil Reservoir rock heterogeneity quantitative estimation from X-ray MCT data. *Energies* **2021**, *14*, 5103. [CrossRef]
21. Peter, J.R.F.; Mike, A.L.; Sarah, J.D. An integrated and quantitative approach to petrophysical heterogeneity. *Mar. Pet. Geol.* **2015**, *63*, 82–96.
22. Chen, H.; Wang, J.; Du, Y. Advances of research methods on reservoir heterogeneity. *Geol. J. China Univ.* **2017**, *23*, 104–116.
23. Zhang, Y.; Tang, Y. A review of reservoir heterogeneity research. *Mar. Geol. Front.* **2011**, *27*, 17–22.
24. Jiao, Y.; Li, S.; Li, Z.; Wen, X. Heterogeneity of porosity and permeability in clastic rock reservoirs. *Oil Gas Geol.* **1998**, *19*, 89–92.
25. Su, P.; Xia, Z.; Wang, P.; Ding, W.; Hu, Y.; Zhang, W.; Peng, Y. Fractal and multifractal analysis of pore size distribution in low permeability reservoirs based on mercury intrusion porosimetry. *Energies* **2019**, *12*, 1337. [CrossRef]
26. Gao, H.; Wang, M.; Shang, S. Quantitative evaluation of micro-pore throat heterogeneity in extra-low permeability sandstone using constant rate mercury penetration: Taking the Chang 8 reservoir of Xifeng oilfield in Ordos Basin. *Prog. Geophys.* **2013**, *28*, 1900–1907.
27. Guo, M.; Zhu, G.; Shou, J.; Xu, X. Feature origin and petroleum explorative significance of crushed fracture in clastic rock. *ACTA Sedimentol. Sin.* **2006**, *24*, 331–340.
28. Giles, M.R. *Diagenesis: A Quantitative Perspective: Implications for Basin Modelling and Rock Property Prediction*; Kluwer Academic Publishers: Dordrecht, The Netherlands, 1997.
29. Luo, M.G. Quantitative models for pore structures of clastic sedimentary rocks. *Acta Pet. Sin.* **1991**, *12*, 27–38.
30. Liu, Y.; Ma, K.; Hou, J.; Yan, L.; Chen, F. Diagenetic controls on the quality of the Middle Permian lucaogou formation tight reservoir, southeastern Junggar Basin, northwestern China. *J. Asian Earth Sci.* **2019**, *178*, 139–155. [CrossRef]
31. Tian, J.; Liu, W.; Wang, F.; Chen, R.; Lin, X. Heterogeneity of the Paleozoic tight sandstone reservoirs in Gaoqiao area of Ordos Basin. *Oil Gas Geol.* **2014**, *35*, 183–189.
32. Cui, J.; Zhu, R.; Wu, S.; Wang, T. Heterogeneity and lower oily limits for tight sandstones: A case study on Chang 7 oil layers of the Yanchang Formation, Ordos Basin. *Acta Pet. Sin.* **2013**, *34*, 877–882.
33. Yue, D.; Lin, C.; Wu, S.; Hou, L. Application of quantitative method for characterizing reservoir heterogeneity to the development of reef limestone reservoir. *Acta Pet. Sin.* **2004**, *25*, 75–79.
34. Feng, C.; Shan, Q.; Shi, W.; Zhu, S. Reservoirs heterogeneity and its control on remaining oil distribution of K1q4, Fuyu oilfield. *J. China Univ. Pet.* **2013**, *37*, 1–7.
35. Hu, R.; Ma, D.; Ma, S.; Yan, B. Identification of flow units and distribution of remaining oil controlled by the architectural structure of point bar. *J. China Univ. Min. Technol.* **2016**, *45*, 135–140.
36. Rasmussen, L.; Fan, T.; Rinehart, A.; Luhmann, A.; Ampomah, W.; Dewers, T.; Heath, J.; Cather, M.; Grigg, R. Carbon storage and enhanced oil recovery in Pennsylvanian morrow formation clastic reservoirs: Controls on oil–brine and oil–Co2 relative permeability from diagenetic heterogeneity and evolving wettability. *Energies* **2019**, *12*, 3663. [CrossRef]
37. Yin, Z.; Lu, G.; Zou, X.; Yang, Z. Heterogeneity of non-marine reservoirs and its influences on recovery factor: Take Gaoshangpu and Yonganzhen oil reservoirs in Jidong and Shengli oilfields as examples. *Oil Gas Geol.* **2006**, *27*, 106–117.
38. Ren, D.; Sun, W.; Zhao, J.; Qu, X.; Zhang, Q. Microscopic waterflooding characteristics of lithologic reservoirs in Ordos Basin and its influence factors: Taking the Chang 81 reservoir in Huaqing oilfield as an example. *J. China Univ. Min. Technol.* **2015**, *44*, 1043–1052.
39. Gharbi, R.; Alajmi, A.; Algharaib, M. The potential of a surfactant/polymer flood in a middle eastern reservoir. *Energies* **2012**, *5*, 58–70. [CrossRef]
40. Lee; Sang, K. Performance of a polymer flood with shear-thinning fluid in heterogeneous layered systems with crossflow. *Energies* **2011**, *4*, 1112–1118. [CrossRef]